Electronic Supplementary Material (ESI) for Journal of Materials Chemistry C.

Electronic Supplementary Information

Synergistic Effect of Zn Doping on Thermoelectric Properties to Realize High Figure-of-merit and Conversion Efficiency in $Bi_{2-x}Zn_xTe_3$ Based Thermoelectric Generator

*Rishikesh Kumar [a, b], Ranu Bhatt [b, *], Arpan Tewary [b], A.K. Debnath [b, f], Pramod Bhatt [c, f], Navaneethan Mani [d], Purushottam Jha [b, f], Pankaj Patro [e, f], Shovit Bhattacharya [b, f], Manbendra Pathak [a], M.K. Khan [a], Ajay Singh [b, f], K.P. Muthe [b]*

[a] Department of Mechanical Engineering, Indian Institute of Technology, Patna-801103, India
[b] Technical Physics Division, Bhabha Atomic Research Centre, Mumbai-400085, India.
[c] Solid State Physics Division, Bhabha Atomic Research Centre, Mumbai-400085, India
[d] Nanotechnology Research Centre (NRC), Faculty of Engineering and Technology, SRM Institute of Science and Technology, Kattankulathur- 603203, India
[e] Power Metallurgy Division, Bhabha Atomic Research Centre, Vashi Complex, Navi Mumbai-400703, India
[f] Homi Bhabha National Institute, Anushaktinagar, Mumbai-400094, India

[*]Corresponding author email id: rbhatt@barc.gov.in

*** Corresponding Author**

Dr. Ranu Bhatt
Scientific Officer
Technical Physics Division
Bhabha Atomic Research Centre, Mumbai, India
Email: rbhatt@barc.gov.in
Ph. No.: +91 22 2558 7084

S1 Module testing unit:

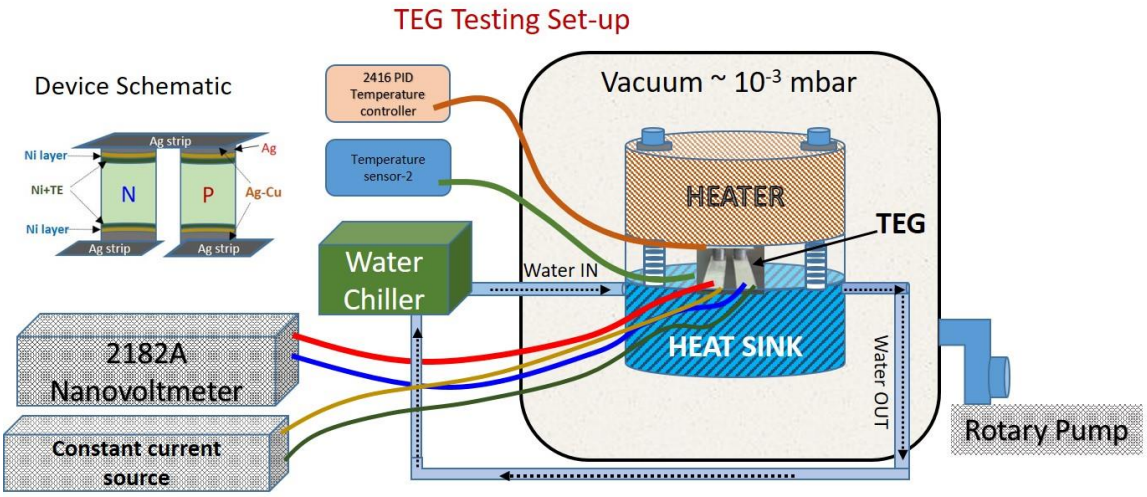

Figure S1: Schematic of TEG and device testing unit

Figure S1 shows the schematic of the TEG and device testing unit. It consists of a top heater controlled using a Eurotherm PID temperature controller, water-cooled heat sink, and measurement system. The hot end temperature is precisely controlled by providing constant power input to the heater. The device is mounted between the heater and heat sink using spring suspension for uniform thermal contact. TEG converts the heat at the hot end to the output power and rejects the rest to the heat sink, maintained near room temperature using forced water cooling. For temperature monitoring, K-type thermocouples are used at hot and cold ends. The device was mounted using silicon heat paste (κ=3.1 W/m-K) to ensure proper thermal contact between the device and the heat transfer layer. The whole assembly is placed inside a chamber which is evacuated using a rotary pump to minimize heat losses during device testing. The device is thermally insulated using a glass wool blanket to reduce heat loss and maximize one-dimensional heat flow. The output voltage and current of the device are

measured using a 2182A nanovoltmeter and a constant current source. The conversion efficiency of the TEG is obtained using the following equation;

$$\eta = \frac{P_{out}}{\dot{Q}} \qquad \text{..... (1)}$$

where $\dot{Q}$ is heat input, which can be estimated using Fourier's law of heat conduction,

$$\dot{Q} = \kappa A \frac{dT}{dx} \qquad \text{..... (2)}$$

Here κ is the thermal conductivity of the material, A is the cross-section of the device, and dt/dx is the temperature gradient across the device. The system was thoroughly calibrated to minimise the heat losses.

S2. Structural analysis using Rietveld refinement of X-ray diffraction pattern:

Table S1: Rietveld refined XRD parameters of $Bi_{2-x}Zn_xTe_3$ (x=0-0.3) powder sample

$Bi_{2-x}Zn_xTe3$												
Atom	Atomic Coordinates				Lattice Parameters				Phase Fraction %		Volume	Fitting Parameters
	x	y	z	Occ	a	b	c	α=β=90				
Bi_1 (6c)	0	0	0.398	0.894	4.3796	4.3796	30.323	γ=120	R-3mH	100	503.64	R_p: 3.43 R_{wp}: 4.39 Chi^2: 1.54 P_h : 0
Bi_2 (6c)	0	0	0.398	0.019								
Te_1 (3c)	0	0	0	0.456								
Te_2 (6c)	0	0	0.792	1.0								
x=0.1												
	x	y	z	Occ	a	b	c	α=β=90	Phase Fract. %		Volume	R_p: 3.39 R_{wp}: 4.36 Chi_2: 1.50 P_h : 0
Bi_1 (6c)	0	0	0.398	0.916	4.3778	4.3778	30.320	γ=120				
Zn_1(6c)	0	0	0.398	0.006					R-3mH	100	503.47	
Te_1 (3c)	0	0	0	0.440								
Te_2 (6c)	0	0	0.792	1.027								
x=0.2												
	x	y	z	Occ	a	b	c	α=β=90	Phase Fract. %		Volume	R_p: 3.37 R_{wp}: 4.32 Chi^2: 1.53 P_h : 0
Bi_1 (6c)	0	0	0.398	0.919	4.379	4.379	30.317	γ=120				
Zn_1(6c)	0	0	0.398	0.005					R-3mH	100	503.6	
Te_1 (3c)	0	0	0	0.424								
Te_2 (6c)	0	0	0.792	1.068								
x=0.3												
	x	y	z	Occ	a	b	c	α=β=90	Phase Fract. %		Volume	R_p: 3.98 R_{wp}: 5.02 Chi^2: 1.58 P_h : 0
Bi_1 (6c)	0	0	0.398	0.920	4.369	4.369	30.242	γ=120				
Zn_1(6c)	0	0	0.398	0.033					R-3mH	100	479.08	
Te_1 (3c)	0	0	0	0.428								
Te_2 (6c)	0	0	0.792	1.056								

S3. X-ray photoelectron spectroscopy measurement

The fitted high-resolution XPS spectra have an average data of nearly 15 scans. The XPS spectra were fitted using XPS-PEAK41 software with two or more peaks and the constraints of full-width half maximum (FWHM) for each peak considered. Fitting was carried out using a combination of Gaussian and Lorentz distribution. Baseline correction was carried out by considering Shirley background in the case of Bi and Tougard background in the case of Te and Zn elements.

S4: Thermoelectric parameters with repetitive thermal cycles

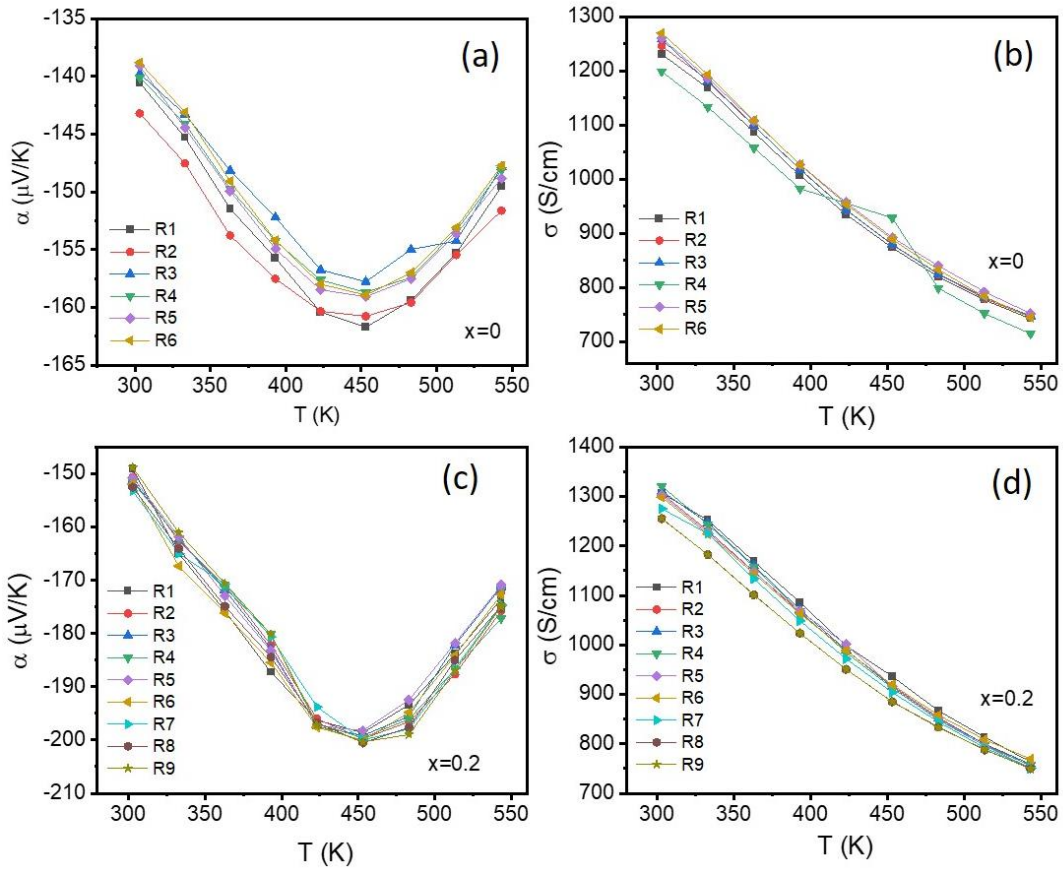

Figure S2. Temperature-dependent Seebeck coefficient and electrical conductivity with repetitive thermal cycles for, (**a-b**) x=0, and (**c-d**) x=0.2, $Bi_{2-x}Zn_xTe_3$ samples.

S5. Lorentz number, phonon thermal conductivity, and bipolar thermal conductivity

The measured total thermal conductivity is expressed as;

$$\kappa = \kappa_{ph} + \kappa_e + \kappa_{bi} \qquad \text{..... (3)}$$

The κ_{bi} of the sample can be estimated from the κ_{ph} (=κ-κ_e) contribution as it includes the portion of bipolar contribution concerning temperature and band structure of the material.

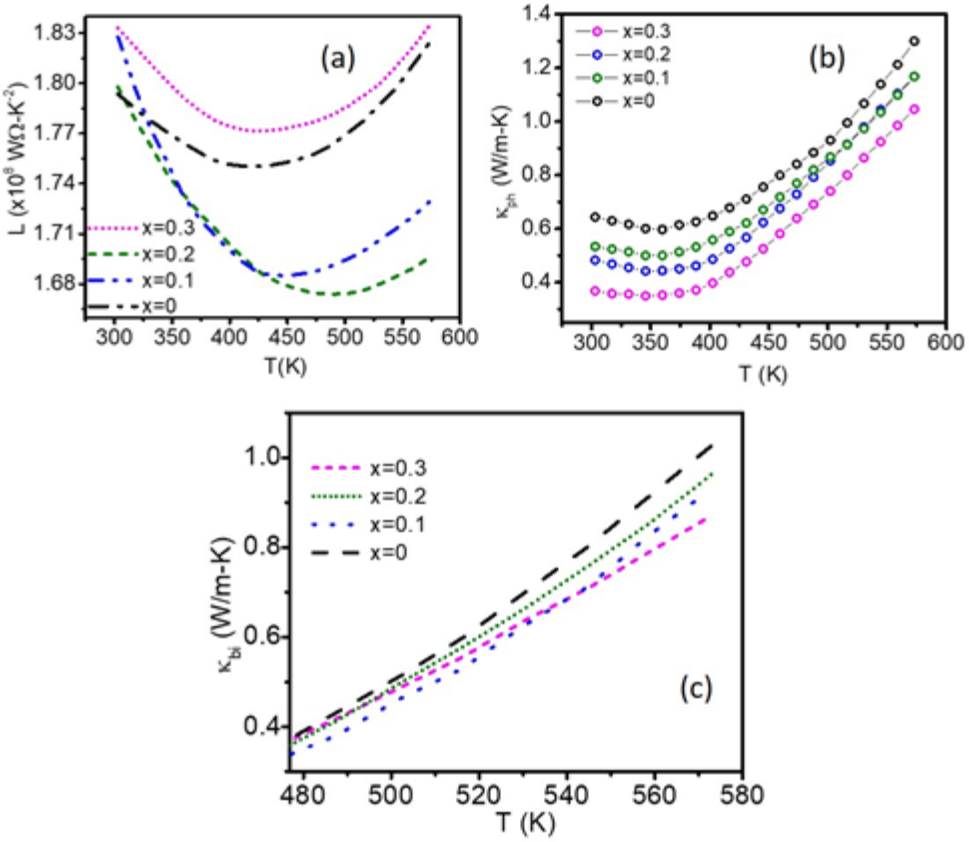

Figure S3: Temperature dependence of (a) Calculated Lorentz factor (*L*), (b) lattice thermal conductivity (κ_{ph}), and (c) temperature dependence of bipolar thermal conductivity (κ_{bi}) for $Bi_{2-x}Zn_xTe_3$ (x=0-0.3) sintered sample.

To calculate κ_e of the material using Weidman Franz relation $\left(\frac{\kappa_e}{\sigma} = L_0 T\right)$, the Lorentz number *L* was estimated by the experimental α value using the relation proposed by Snyder et al. [1];

$$L = 1.5 + \exp\left[-\frac{|\alpha|}{116}\right] \qquad \text{..... (4)}$$

For single parabolic band (SPB), numerically, both *L* and *α* can be expressed in terms of reduced chemical potential (*ξ*) and carrier scattering factor (*S*) as given below [2-3];

$$L = \left(\frac{k_B}{e}\right)^2 \frac{(1+S)(3+S)F_S(\xi)F_{S+2}(\xi) - (2+S)^2 F_{S+1}(\xi)^2}{(1+S)^2 F_S(\xi)^2} \qquad \text{..... (5)}$$

$$\alpha = \frac{k_B}{e}\left(\frac{(2+S)F_{S+1}(\xi)}{(1+S)F_S(\xi)} - \xi\right) \qquad \text{..... (6)}$$

Where F_j (ξ) represents Fermi integral

$$F_j(\xi) = \int_0^\infty \frac{\varepsilon^j d\varepsilon}{1 + Exp[\varepsilon - \xi]} \qquad \text{..... (7)}$$

By assuming the acoustic phonon scattering as the dominant scattering mechanism, *L* is estimated using equation 4. Figure S3 (a) shows the temperature dependence of *L* for different Zn content. The κ_{ph} is calculated using eq. 3, shown in fig. S3 (b). A sudden rise in κ_{ph} beyond 400 K is due to bipolar contribution due to minority charge carriers. The calculated κ_{bi} with temperature for different Zn content is shown in fig. S3 (c).

S5. Material synthesis and thermoelectric properties of $Bi_{0.5}Sb_{1.495}Cu_{0.005}Te_3$

For material synthesis, high purity elements of Bi (99.999%), Te (99.999%), Cu (99.999%), and Sb (99.999%) were sealed in evacuated (10^{-5} Torr) quartz ampoule according to the stoichiometry. The material was melted in a rocking furnace at 1023 K for 8 hours. For uniform mixing, the ampoule was rocked at an angle of 45° for 5 hours. The obtained ingot was then crushed in a ball mill at 300 RPM for 2 hours and then sintered at 723 K for further

characterization. Figure S4 shows the thermoelectric parameters of the sintered sample. Temperature-dependent resistivity shows the metallic trend, in addition to increasing positive α value with temperature suggesting *p*-type conduction in the sample, which attains a

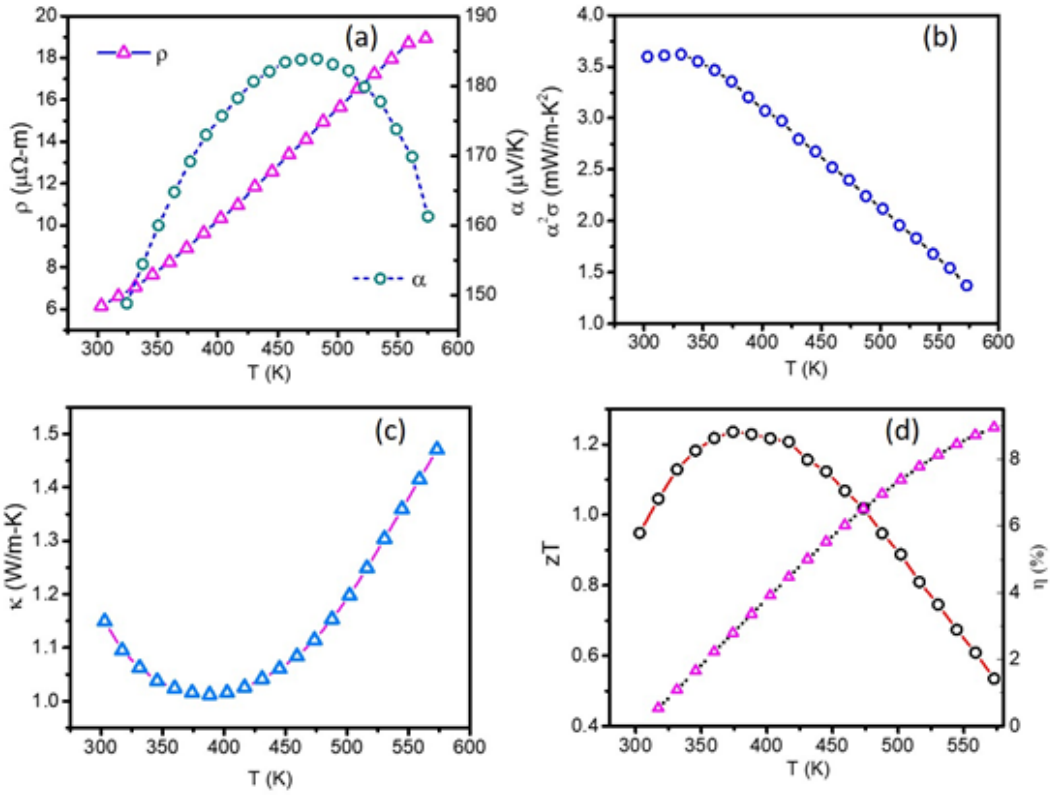

Figure S4: Temperature dependence (a) electrical resistivity and Seebeck coefficient, (b) power factor ($\alpha^2\sigma$), (c) thermal conductivity, and (d) dimensionless figure-of-merit and theoretical efficiency of sample $Bi_{0.5}$ $Sb_{1.495}Cu_{0.005}Te_3$ sample.

maximum value of ~185 μV/K, at 573 K. Sample interestingly shows a maximum power factor value of 3.7 mW/m-K^2 at 323 K. Thermal conductivity of the sample varies in the range of 1.15 W/m-K to 1.45 W/m-K in the measured temperature range. In the sample, a maximum *zT* of ~1.2 is achieved between 373 K -423 K. Theoretically, it is possible to achieve ~ 9 % conversion efficiency in this material at T_H and T_c of 573 K and 303 K, respectively.

S7. Finite element analysis of unicouple device using COMSOL Multiphysics software.

The power generation characteristic of the unicouple module was simulated with the three-dimensional finite-element analysis using COMSOL Multiphysics software. For simulation the measured experimental thermoelectric parameters of *n*-type ($Bi_{1.8}Zn_{0.2}Te_3$) and *p*-type ($Bi_{0.5}Sb_{1.495}Cu_{0.005}Te_3$) were used. The thermoelectric effect in a steady state can be expressed using the following equations [4-6];

Electrical current density (*J*) $$J = \sigma\left(-\nabla V - \alpha\nabla T\right)$$ ..... (8)

Heat flux (*q*) $$q = -\kappa\nabla T$$ ..... (9)

$$\nabla J = 0$$ ..... (10)

$$\nabla\left(\kappa\nabla T\right) + \frac{J^2}{\sigma} - TJ\nabla\alpha = 0$$ ..... (11)

The simulation of *J*, *q*, *V*, and *T* was carried out considering electrical and thermal boundary conditions. The input geometry of the module is kept similar to the experimental module. Figure S5 shows the simulated V_L, P_{out}, and η as a function of ΔT. For ΔT of ~220 K, the

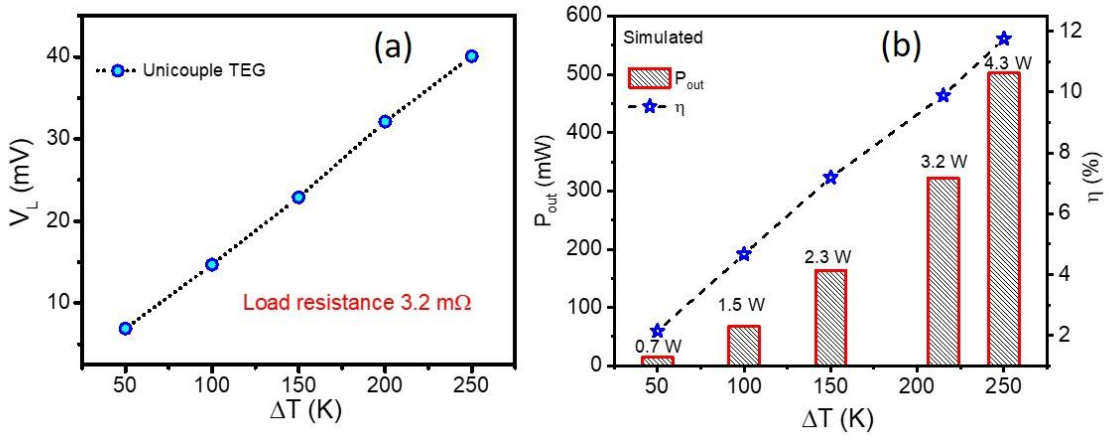

Figure S5. (a) COMSOL simulated graph of unicouple TEG; (a) shows temperature dependence load voltage (V_L) at load resistance and (ii) power output (P_{out}) and conversion efficiency (η) as a function of temperature gradient (ΔT). The value above the bar represents the simulated power input for corresponding ΔT.

simulated maximum P_{out} of ~325 mW is observed, which shows η of ~ 10.2 % at simulated heat input of 3.2 W.

Supplementary References

1. A. Putatunda, D.J. Singh, *Materials Today Physics,* 2019*,* **8**, 49e55.
2. A. F. May, J.-P. Fleurial and G. J. Snyder, *Phys. Rev. B: Condens. Matter Mater. Phys*., 2008, **78**, 125205.
3. S. Johnsen, J. He, J. Androulakis, V. P. Dravid, I. Todorov, D. Y. Chung and M. G. Kanatzidis, *J. Am. Chem. Soc.,* 2011, **133**, 3460–3470.
4. X. K. Hu, A. Yamamoto, M. Ohta, H. Nishiate, *Rev. Sci.Instrum.,* 2015, **86**, 045103.
5. X. K. Hu, H. Takazawa, K. Nagase, M. Ohta, A. Yamamoto, *J. Electron. Mater.,* 2015, **44**, 3637–3645.
6. B. Sherman, R. R. Heikes and R. W. Ure, *J. Appl. Phys.,* 1960, **31**, 1–16.